ORIGINAL ARTICLE

lajss.org Latin American Journal of Solids and Structures

www.lajss.org

Study on cone angle of shockwave front in liquid composite protective structure

You-er Cai[a], Yaping Tan[b], Xudong Zu[a], Zhengxiang Huang[a]*, Xiaojun Shen[a,c], Xin Jia[a], Qiangqiang Xiao[a]

[a] School of Mechanical Engineering, Nanjing University of Science and Technology, Nanjing 210094, China. Emails: caiyouer@njust.edu.cn; zuxudong9902@njust.edu.cn; huangyu@njust.edu.cn; sxj_1959@126.com; jiaxin@mail.njust.edu.cn; xiao_wawj@njust.edu.cn

[b] School of Information Technology, Jiangsu Open University, 399 Jiangdong North Road, Nanjing 210036, China. Email: 315101002424@njust.edu.cn

[c] Unit 63961 Peoples Liberation Army 6th Beiyuan Road, Chaoyang Beijing, 10012, China. Email: sxj_1959@126.com

*Corresponding author

https://doi.org/10.1590/1679-78258026

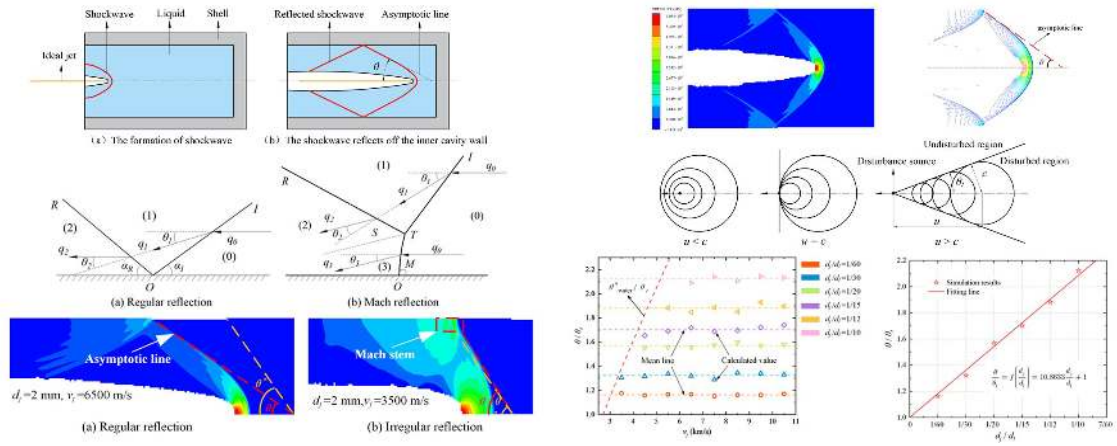
Abstract

Liquid composite armor has demonstrated excellent performance in protecting against shaped charge jets. Currently, most existing theoretical calculation models for the velocity range of the disturbed jet approximate the cone angle of the shockwave front as the Mach angle. However, indiscriminately equating the cone angle of the shockwave front with the Mach angle can lead to significant errors in the calculated velocity range of the disturbed jet. To address this issue, this study focuses on investigating the variation of the cone angle of the shockwave front within the liquid composite protective structure. Firstly, a dimensional analysis was conducted to determine the functional relationship between the cone angle of the shockwave front and relevant parameters. Then, the process of jet penetrating liquid composite protective structure was simulated by Autodyn. The results demonstrated that the normalized cone angle solely depends on the normalized diameter within the critical angle. By fitting the simulation data, the formula for calculating the cone angle of the shockwave front was derived.

Keywords

Shockwave, Liquid composite protective structure, Shaped charge jet, Numerical simulation, Dimensional analysis, Mach angle

Graphical abstract



Received: February 06, 2024. In revised form: February 14, 2024. Accepted: February 14, 2024. Available online: February 20, 2024.
https://doi.org/10.1590/1679-78258026

Latin American Journal of Solids and Structures. ISSN 1679-7825. Copyright © 2024. This is an Open Access article distributed under the terms of the Creative Commons Attribution License, which permits unrestricted use, distribution, and reproduction in any medium, provided the original work is properly cited.

1 INTRODUCTION

The relationship between warhead damage technology and armor protection technology is like that of a 'spear' and a 'shield', mutually opposing but also developing together. Since the 1980s, the development of high-tech military technology has significantly improved the comprehensive protection performance of tanks and revolutionized traditional anti-tank weapon systems (Cao et al. 2019). By harnessing the shaped charge effect, high-speed metal jets generated by shaped charges can reach speeds exceeding 10 km/s. Furthermore, with the widespread use of new high-energy explosives, precise propellant manufacturing techniques, and increased propellant load, the most modern high explosive anti-tank missiles can obtain a penetration capability of up to 1500 mm of RHA (Żochowski and Warchoł 2023, Williams and Dhingra 2016), posing a major threat to tanks and armored vehicles on the battlefield (Huang 2014). Armor serves as one of the primary means for tanks and armored vehicles to ensure their survival on the battlefield (Zhang et al. 2000). In response to the rapid development of anti-armor weapons, countries worldwide have made continuous efforts to develop armor protection technology, aiming to enhance survivability and combat capabilities on the battlefield (Zhang et al. 2014). Various types of armor, including homogeneous armor, spaced armor, ceramic composite armor, explosive reactive armor, rubber composite armor, and electromagnetic armor, have been successively developed and applied.

As a novel form of passive protective armor, liquid-filled composite armor displays a distinctive protection mechanism that sets it apart from other passive protective systems. It counters shaped charge jets by utilizing the radial backflow of liquid propelled by shockwave propagation, effectively overcoming rigidity with flexibility. Liquid-filled composite armor possesses several advantages, including high anti-penetration performance and minimal collateral damage. The introduction of liquid honeycomb composite armor on Ukraine's main battle tank, 'Fortress M', has sparked academic and research interest in understanding the interference mechanism of liquid composite protective structures against shaped charge jets. As early as 1981, White and Wahll conducted experiments to study the process of jet penetration into airtight structures filled with water or other liquids (White and Wahll 1981). They demonstrated that liquid-filled airtight structures exhibited strong resistance against jet penetration. In recent years, Gao et al. have developed theoretical models based on the virtual origin theory and shockwave propagation theory to analyze the interference effects of enclosed liquid-filled composite structures on shaped charge jets. They have calculated the range of disturbance velocities caused by the radial convergence of liquid propelled by sidewall-reflected shockwaves (Gao et al. 2016a, Gao et al. 2016b). Zhang et al. have further improved and refined the theoretical model for jet penetration into single-cell liquid-filled structures, focusing on the direction of shockwave propagation, propagation path, and reflection mode. Zhang proposes that the interference of liquid on jet stability originates from both the radial convergent backflow of the liquid and the liquid spray (Zhang et al. 2017). Tan and Zu conducted dimensional analysis and static jet impact tests to investigate the relationship between the residual penetration capability of a shaped charge jet and the sound speed, viscosity, and density of the liquid (Tan et al. 2019, Zu et al. 2019). Guo et al. considered the multiple impacts of the jet on the liquid and proposed that the liquid backflow caused by bottom reflection and cavity wall reflection interfered with the middle and rear segments of the shaped charge jet, respectively. They utilized the lateral velocity method to calculate the residual penetration depth of the jet after being disturbed by the liquid composite armor (Guo et al. 2018, Guo et al. 2019). Zu et al. analyzed the lateral migration of the disturbed jet and the lateral velocity generated by the breakup of the jet at a high standoff distance. They calculated the variation in velocity range of the disturbed jet and the penetration capability of the residual jet at different impact angles (Zu et al. 2021). Taking into account the compressibility of the liquid, Cai et al. conducted a theoretical analysis on the process of center/eccentric jet penetration into liquid com00posite armor, and analyzed the propagation of shockwave and the backflow process of liquid particles by using AUTODYN. Their findings concluded that the interference of liquid composite armor on the jet includes sidewall reflection interference, bottom reflection interference, and sidewall secondary reflection interference (Cai et al. 2021, Cai et al. 2022).

Liquid composite armor has demonstrated excellent performance in protecting against shaped charge jets. Previous studies have indicated that the shockwave generated during jet penetration plays a crucial role in the backflow of liquid within the cavity, thereby interfering with the jet. The propagation characteristics of the shockwave directly impact the effectiveness of the armor. Currently, most existing theoretical calculation models for the velocity range of the disturbed jet approximate the cone angle of the shockwave front as the Mach angle, without studying the variation of the cone angle of the shockwave front within the liquid composite protective structure and its difference from the Mach angle. However, the variation of the cone angle of the shock wave front is influenced by factors such as the propagation distance of the shockwave, the diameter of the shaped charge jet, and boundary effects, and it cannot be simply equated with the Mach angle. Indiscriminately approximating the cone angle of the shockwave front to the Mach angle can result in significant errors in the calculated velocity range of the disturbed jet, which is not conducive to the design work of liquid composite protective structures. To address this issue, this study focuses on researching the variation of the cone angle

of the shockwave front within the liquid composite protective structure. Firstly, the propagation characteristics of disturbance in the medium and the reflection types of the shockwave on solid walls were introduced. Next, a dimensional analysis was conducted to investigate the process of jet penetration into the liquid composite protective structure. This analysis determined the functional relationship between the cone angle of the shockwave front and relevant parameters. Subsequently, the AUTODYN software was utilized to simulate the process of a constant-speed projectile penetrating the liquid composite protective structure. The simulation results provided insights into the relationship between the cone angle of the shockwave front and the velocity and diameter of the projectile. It was observed that the normalized cone angle of the shockwave front θ/θ_t varied solely based on the normalized diameter d_j/d_l within the critical incident angle θ^*. The reliability of the simulation method was confirmed through comparisons the confirmatory simulation results with relevant test results. Finally, a calculation formula for determining the cone angle of the shockwave front was developed by fitting the simulation data.

2 PROPAGATION CHARACTERISTICS OF SHOCKWAVE IN LIQUID COMPOSITE PROTECTIVE STRUCTURE

2.1 Propagation of the initial shockwave in liquid

According to the basic principles of fluid dynamics, the propagation characteristics of disturbances are influenced by the velocity of the disturbance source in the liquid, as shown in Figure 1. When the ratio of the velocity of the disturbance source u to the sound velocity of the liquid c is less than 1 (i.e., $M < 1$), the disturbance will propagate throughout the entire flow field. When the velocity of the disturbance source u is equal to the sound velocity of the liquid c (i.e., $M = 1$), the disturbance will be confined to the region behind the boundary line perpendicular to the direction of motion of the disturbance source. However, when the ratio of the velocity of the disturbance source u to the sound velocity of the liquid c is greater than 1 (i.e., $M > 1$), the disturbance will be confined to a conical envelope. In this case, the disturbance source is located at the vertex of the cone, and the angle between the generatrix of the cone and the direction of motion of the disturbance source is called the Mach angle. The Mach angle θ_t satisfies the equation:

$$\sin\theta_t = \frac{c}{\mathrm{u}} = \frac{1}{M} \tag{1}$$

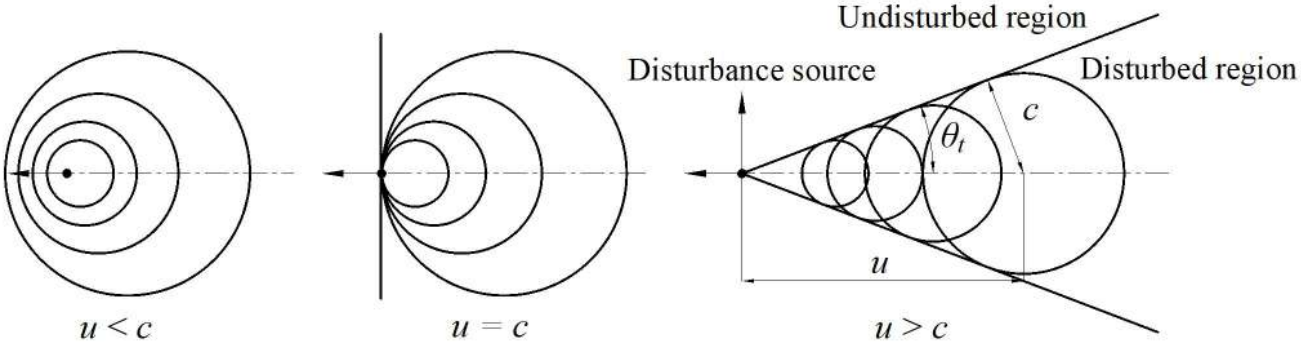


Figure 1 Propagation characteristics of disturbance in fluids

When a high-velocity jet penetrates into a liquid, it generates a shockwave in the liquid. Held conducted experiments to measure the evolution of shockwaves in water during the process of jet penetration at different velocities (Held et al. 1996). It was observed that the shockwave formed during the high-velocity jet impact on the liquid has a bow-shaped profile. It was also found that when the propagation distance is far where the expansion only takes place at sound velocity c, the relationship between the shockwave cone angle, liquid sound velocity, and jet penetration velocity can be described using Equation (2):

$$\theta_t = \arcsin\left(\frac{c}{\mathrm{u}}\right) \tag{2}$$

However, in the case of shockwave propagation in the liquid during jet penetration into a liquid composite protective structure (as shown in Figure 2), various factors come into play. These factors include the relatively short propagation distance of the shockwave and the presence of boundary effects within the liquid cavity. As a result, there can be significant differences between the cone angle of the shockwave front and the Mach angle. Therefore, a detailed analysis is required to accurately calculate the cone angle of the shockwave front.

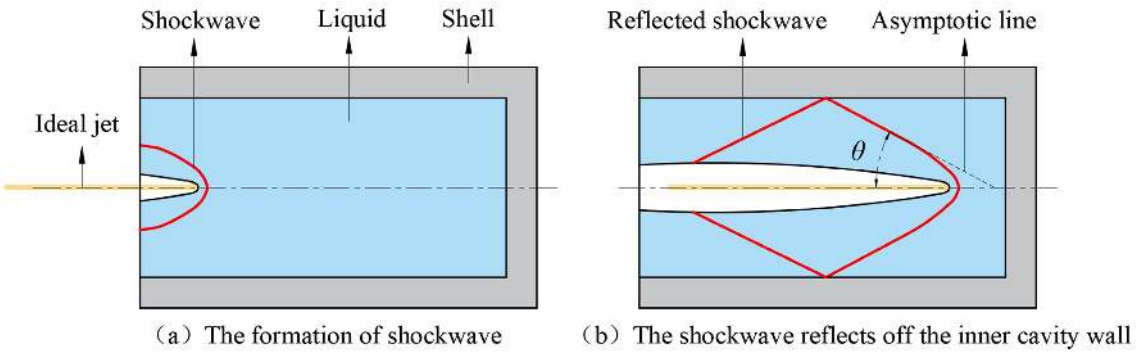


Figure 2 Propagation of shockwave in a liquid composite protective structure

2.2 Characteristics of shock wave reflection on wall surface

Shock reflection can be categorized into regular reflection and irregular reflection (Mach 1878). Irregular reflection further consists of Mach reflection and weak shock reflection. The shock reflection relationships for regular reflection and Mach reflection are depicted in Figure 3.

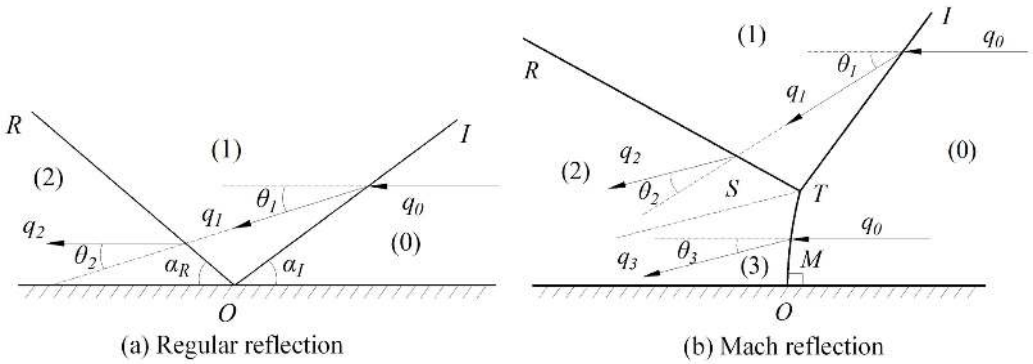


Figure 3 *Diagram of shock reflection relationship* (Ben-Dor 2007, Vasilev et al. 2008)

According to the solution method of the shock polar diagram (Mach 1878, Kawamura and Saito 1956) and the detachment criterion (Ben-Dor 2007, Yang et al. 2012), it can be seen that the regular reflection of an oblique shockwave on a rigid wall only occurs when the incidence angle of the shockwave does not exceed the theoretical critical angle. When the incident angle of shockwave is greater than the theoretical critical angle, the solution of the shock polar curve equation no longer satisfies both the oblique shockwave condition and the solid wall condition. As a result, the shockwave will be irregularly reflected on the wall. Due to the effect of irregularly reflected shockwaves, liquid particles generate a velocity component directed towards the wall, as depicted in Figure 3(b). The presence of this velocity component is unfavorable for the radial convergence of the liquid to interfere with the shaped charge jet. To prevent irregular reflection of shockwaves on the wall surface caused by excessively large incident angles, it is crucial to design the dimensions of the liquid composite protective structure in an optimal manner. This involves ensuring that the dimensions are carefully optimized to minimize the risk of irregular reflection occurring when the shockwave interacts with the wall surface. In this paper, only the variation of the shockwave cone angle was discussed when the incident angle of the shockwave is within the critical angle range.

For shockwaves in condensed medium, there is

$$\sin\theta^* = \sqrt{\frac{\lambda}{2\lambda - 1}} \tag{3}$$

Where, θ^* represents the critical incident angle at which the shockwave regularly reflects off a solid wall, λ is the Hugoniot constant for the condensed medium. For water, $\lambda = 1.921$. Hence, the critical incident angle at which the shockwave regularly reflects in water can be calculated.

$$\theta^*_{water} = \arcsin\sqrt{\frac{\lambda}{2\lambda - 1}} = 55.3^\circ \tag{4}$$

Therefore, in order to prevent the shockwave in water from undergoing irregular reflection on the inner wall surface, the cone angle of the shockwave front θ needs to satisfy $0 < \theta \leq \theta^*_{water}$.

3 DIMENSIONAL ANALYSIS

According to the theoretical model proposed (Cai et al. 2021), several key physical parameters are related to the cone angle of the shockwave front during the penetration process of a liquid composite protective structure by a jet. These parameters are presented in Table 1 and encompass six physical quantities related to the macroscopic objects of the jet, liquid, and liquid composite structure. The symbols, dimensions, and units corresponding to these quantities are provided in Table 1. It should be noted that due to the presence of diameter and velocity gradients at the head and tail of the jet, the jet diameter and velocity mentioned here refer to the instantaneous values corresponding to the penetration process.

Table 1 Parameters of key physical quantities

Object	Quantity	Symbol	Dimension	Unit
Shaped charge jet	Velocity	v_j	LT^{-1}	m/s
	Diameter	d_j	L	m
	Density	ρ_j	ML^{-3}	kg/m^3
Liquid	Density	ρ_l	ML^{-3}	kg/m^3
	Sound velocity	c_l	LT^{-1}	m/s
Liquid composite protective structure	Diameter of inner cavity	d_l	L	m

The relationship between the cone angle of the shockwave front and the independent variables was discussed. The unknown function representing the cone angle of the shockwave front θ with respect to the six independent variables mentioned in Table 1 is denoted as

$$\theta = f\left(v_j, d_j, \rho_j, \rho_l, c_l, d_l\right) \tag{5}$$

Where, f represents some functional relationship. Taking ρ_l、c_l and d_l as the basic quantities, the following formula can be obtained

$$\theta = f\left(\frac{v_j}{c_l}, \frac{d_j}{d_l}, \frac{\rho_j}{\rho_l}, 1, 1, 1\right) \tag{6}$$

That is,

$$\theta = f\left(\frac{v_j}{c_l}, \frac{d_j}{d_l}, \frac{\rho_j}{\rho_l}\right) \tag{7}$$

Since the penetration velocity satisfies $u = \dfrac{v_j}{1+\sqrt{\rho_l/\rho_j}}$, equation (7) can be transformed into

$$\theta = f\left(\frac{c_l}{u}, \frac{d_j}{d_l}\right) \tag{8}$$

Assuming that $f\left(d_j/d_l\right)$ and $g\left(c_l/u\right)$ are mutually independent, we have

$$\theta = f\left(\frac{d_j}{d_l}\right) g\left(\frac{c_l}{u}\right) \tag{9}$$

Obviously, $g\left(c_l/u\right)$ corresponds to the Mach angle $\theta_t = \arcsin\left(c_l/u\right)$. Therefore, Equation (9) can be transformed into

$$\frac{\theta}{\theta_t} = f\left(\frac{d_j}{d_l}\right) \tag{10}$$

It can be observed that when the assumption is valid, the normalized cone angle $\theta \,/\, \theta_t$ is solely determined by the normalized diameters d_j/d_l. The following text will validate this assumption.

4 SIMULATION ANALYSIS

To mitigate errors arising from the attenuation of jet penetration velocity, this study employed the AUTODYN solver to numerically simulate the process of a projectile penetrating a liquid composite protective structure at a constant velocity. AUTODYN is a numerical simulation software that utilizes the explicit finite element method and is frequently used for simulating and calculating problems related to high-speed impacts (Zhu et al. 2019) shaped charge jet formation (Gu et al. 2022, Shi et al. 2023) and wave propagation (Zhang et al. 2023, Yang et al. 2023). Through simulation, the propagation process of the shockwave in the liquid during the projectile's penetration into the liquid composite protective structure was obtained.

4.1 Modeling process

To reduce computational time and considering that the model is a solid of revolution, this study adopts a 2D model for numerical simulation. The simulation model consists of a projectile, a metal shell, and a liquid. High-conductivity oxygen-free copper is chosen as the projectile material, steel Q235 is selected as the shell material, and water is used as the liquid material. The Euler-Lagrange coupling algorithm is used to compute the penetration process of a projectile at a constant velocity into a liquid composite protective structure. Figure 4 depicts the finite element model. In this model, the Euler part is filled with the projectile and the liquid, while the Lagrange part is filled with the metal shell. The diameter of the internal cavity filled with liquid d_l is 30 mm, with a length h_l of 145 mm. Both the length of the projectile l_j and the length of the shell h_t are 150 mm. To approximate the side shell of the liquid composite protective structure as a rigid wall and minimize its deformation during jet impact, the thickness of the shell is set to 65 mm.

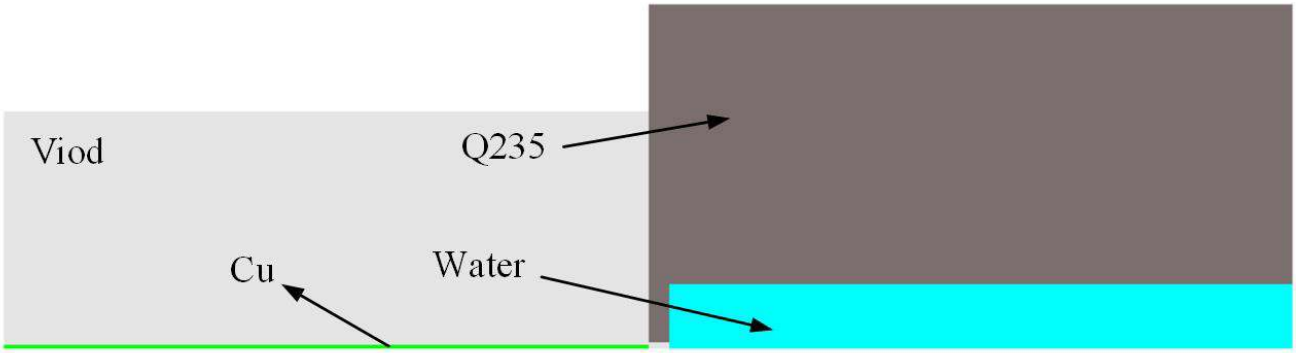


Figure 4 Schematic diagram of simulation model

In the simulation model, both the Euler and Lagrange parts are chosen to have a uniform square grid. The sensitivity of the mesh size was studied through the application of 1, 0.5, 0.25 and 0.1 mm meshes in the numerical calculation. The calculation shows that the results were significantly different with mesh size reduction from 1 mm to 0.25 mm, while the results stabilized when the mesh size reduced from 0.25 mm to 0.1 mm. Thus, it was determined that the grid size should be set to 0.25 mm × 0.25 mm in order to achieve the desired level of computational accuracy while maintaining computational efficiency.

Table 2 Material models

No.	Material	Strength model	State equation
1	Water	None	Shock
2	Q235	Johnson Cook	Shock
3	Cu	Steinberg Guinan	Shock

The material models selected are as shown in Table 2. The state equation of water, steel Q235 and Cu all adopted the shock equation, and the Shock EOS can be expressed as (Ansys Inc 2022)

$$P = P_H + \Gamma\rho\left(e - e_H\right) \tag{11}$$

Where $\Gamma\rho = \Gamma_0\rho_0 = \text{constant}$ is assumed and

$$P_H = \frac{\rho_0 c_0^2 \mu\left(\mu + 1\right)}{\left[1 - \left(\lambda - 1\right)\mu\right]^2} \tag{12}$$

$$e_H = \frac{1}{2}\frac{P_H}{\rho_0}\left(\frac{\mu}{1+\mu}\right) \tag{13}$$

Where μ is the compression ratio defined as $\mu = \left(\rho/\rho_0 - 1\right)$, ρ is the current density of the material and ρ_0 is the initial density of the material. The initial sound speed of water c_{l0} is 1647 m/s, and the initial density of water ρ_{l0} is 998 kg/m^3.

The strength model of steel Q235 adopted the Johnson-Cook model, the model for the von Mises flow stress (σ) being expressed as

$$\sigma = \left(A + B\varepsilon_p^n\right)\left(1 + C\ln\varepsilon_p^*\right)\left(1 - T_H^m\right) \tag{14}$$

Where A, B, n, m, and C denote the initial yield stress, strain strengthening coefficient, strain strengthening index, temperature softening index, and strain rate strengthening coefficient of the material, respectively (Johnson and Cook 1983). The material parameters of steel Q235 are listed in Table 3.

Table 3 Material parameters of steel Q235

ρ (kg/m³)	G (Gpa)	T_m (K)	T_R (K)	A (Gpa)	B (Gpa)
7830	77	1793	300	0.352	0.300
n	m	C	S_1	c_1 (m/s)	γ_0
0.26	1.03	0.014	1.49	4569	2.17

The strength model of Cu adopted the Steinberg-Guinan model. The constitutive relations for shear modulus G and yield stress Y for high strain rates are

$$G = G_0\left[1+\left(\frac{G_P'}{G_0}\right)P\eta^{-1/3}-\left(\frac{G_T'}{G_0}\right)\left(T-300\right)\right] \tag{15}$$

$$Y = Y_0\left[1+\left(\frac{Y_P'}{Y_0}\right)P\eta^{-1/3}-\left(\frac{G_T'}{G_0}\right)\left(T-300\right)\right]\left(1+\beta\varepsilon\right)^n \tag{16}$$

Where, ε is the effective plastic strain, η is the compression, T is the temperature, and the primed parameters with the subscripts P and T are derivatives of that parameter with respect to pressure and temperature at the reference state ($T=300\,\mathrm{K}$, $P=0$, $\varepsilon=0$) (Steinberg et al. 1980). The subscript zero also refers to values of G and Y at the reference state. The material parameters of Cu are listed in Table 4.

Table 4 Material parameters of Cu

ρ (kg/m³)	G (Gpa)	T_m (K)	Y (Gpa)	$Y_{\max}$ (Gpa)
8930	47.7	1793	0.120	0.640
β	n	G_P'	G_T' (Gpa/K)	Y_P'
36	0.45	1.35	-0.01798	0.003396

In order to verify the relationship between the normalized cone angle $\theta\,/\,\theta_t$ and the normalized diameter d_j/d_l, the initial conditions of the simulation were set. Taking into account the commonly used jet forming parameters for armor-piercing warheads, this study sets the velocity range of the projectile from 2500 m/s to 10500 m/s. Additionally, while keeping the cavity diameter constant, the range of jet diameters is set from 0.5 mm to 6 mm to obtain different normalized diameter d_j/d_l. The simulation scheme is summarized in Table 5.

Table 5 Simulation scheme

parameter	Radius of projectile d_j (mm)	Velocity of projectile v_j (m/s)
Value	0.5, 1, 1.5, 2, 2.5, 3, 4, 5, 6	2500, 3500, 4500, 5500, 6500, 7500, 8500, 9500, 10500

4.2 Reliability verification of simulation methods

To validate the reliability of the simulation results, this study refers to relevant experiments (Held 1995). By using a constant velocity projectile as a substitute for the shaped charge jet generated by KB 44 shaped charge, the propagation of shockwave generated by jet penetrating water with different velocity and diameter is simulated. The obtained statistical relationship between the propagation position and time of the shockwave is compared with experimental results to validate the reliability of the simulation method used in this study.

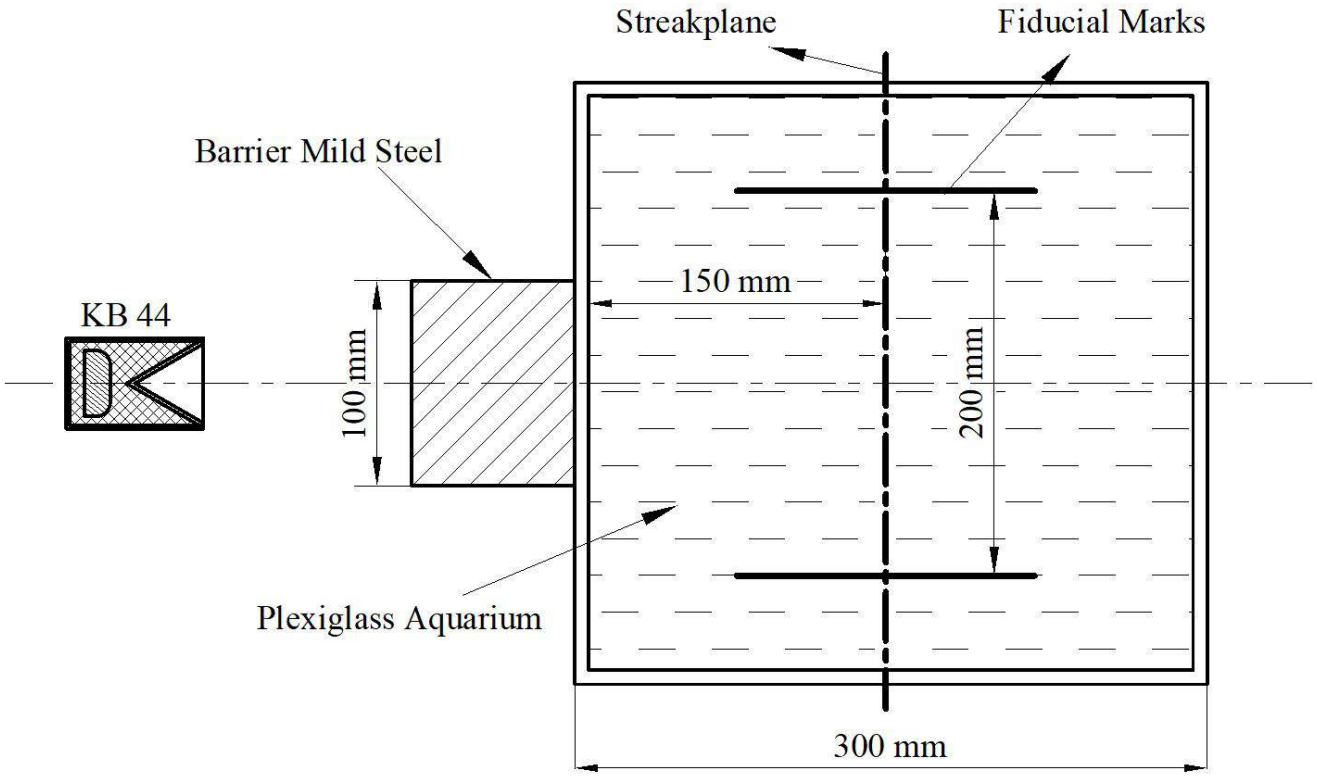


Figure 5 The layout of the experiment (Held 1995)

The experiment layout is shown in Figure 5. The head jet was consumed by a front barrier mild steel, and the motion velocity when the jet penetrated to the streak plane of the water tank was adjusted by controlling the thickness of the baffle. Simultaneously, a high-speed imaging system was used to capture the expansion of the jet reaming and the propagation of the shockwave. This allowed for obtaining the variations in the radial reaming diameter of the jet and the diameter of the shockwave front over time at the streak plane. As shown in Table 6, this study selected the following operating conditions as comparison objects. By comparing the simulation data of the shockwave diameter variation over time with experimental data, the reliability of the simulation method was validated.

Table 6 Scheme of verification simulation

No.	1	2	3	4
Radius of projectile r_j (mm)	0.82	0.96	1.15	1.5
Velocity of projectile v_j (m/s)	6000	5000	4000	3000

The simulation model, as depicted in Figure 6, incorporates water, plexiglass, and high-conductivity oxygen-free copper as materials, selected from the AUTODYN material library. Due to the large size of the model and the long computation time involved, as well as the focus on a specific region along the longitudinal axis as the key data acquisition area, a graded mesh approach was employed for the verification simulation. The refined mesh was applied only in the key areas of interest. In the Eulerian part of the model, the axial grid size was set to 0.5 mm, while the radial refined mesh had a size of 0.2 mm. The graded mesh exhibited a size range of 0.2 mm to 1.2 mm, as illustrated in Figure 7. The remaining modeling processes and methods remained consistent with the other simulations conducted in this study.

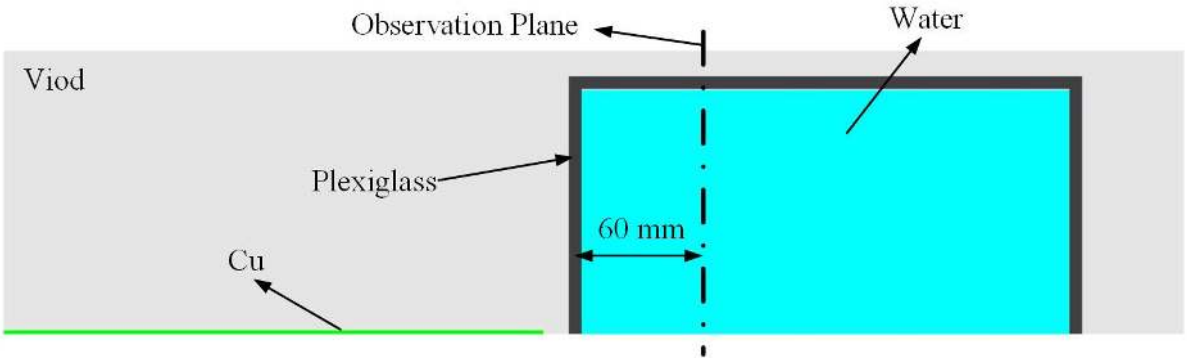


Figure 6 Schematic diagram of verification simulation model

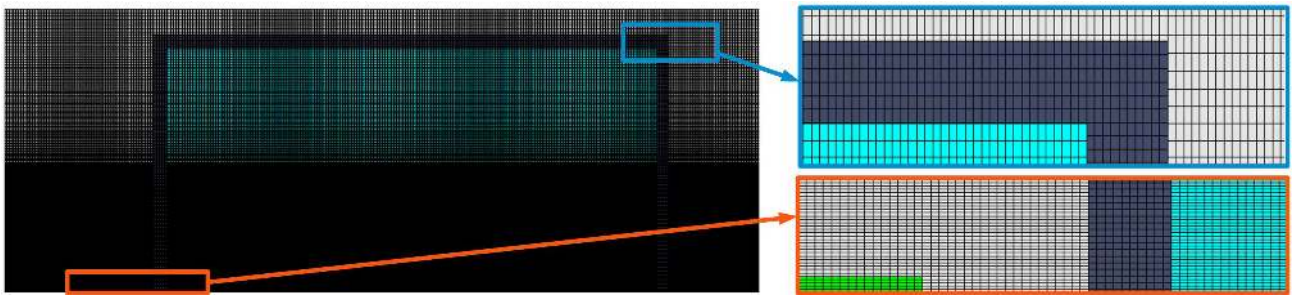


Figure 7 Part of the simulation grid

A plane situated at a distance of 60 mm from the water tank wall was selected as the observation plane. The initial time was defined as the moment when the shockwave began propagating towards the observation plane. At various relative times, the diameters of the shockwave front were measured and obtained for comparison with experimental results (Held 1995). Figure 8 illustrates that the simulated variations in the radial diameter of the shockwave front over time closely align with the experimental results. This finding suggests that the simulation method employed in this study is suitable for analyzing the propagation of the shockwave in the liquid during the penetration of a liquid composite protective structure by a high-velocity projectile.

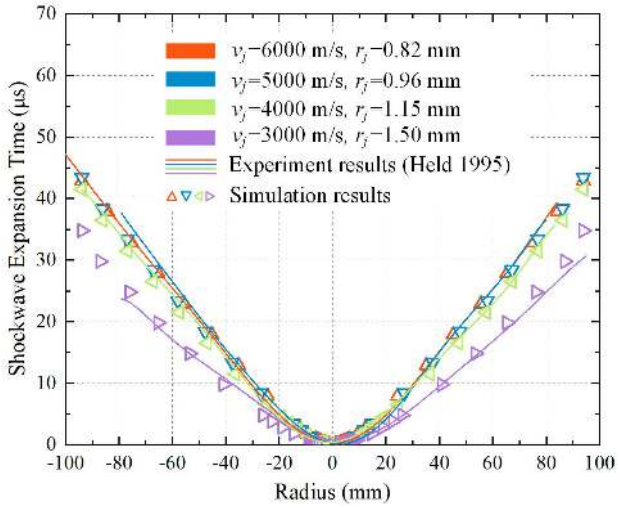
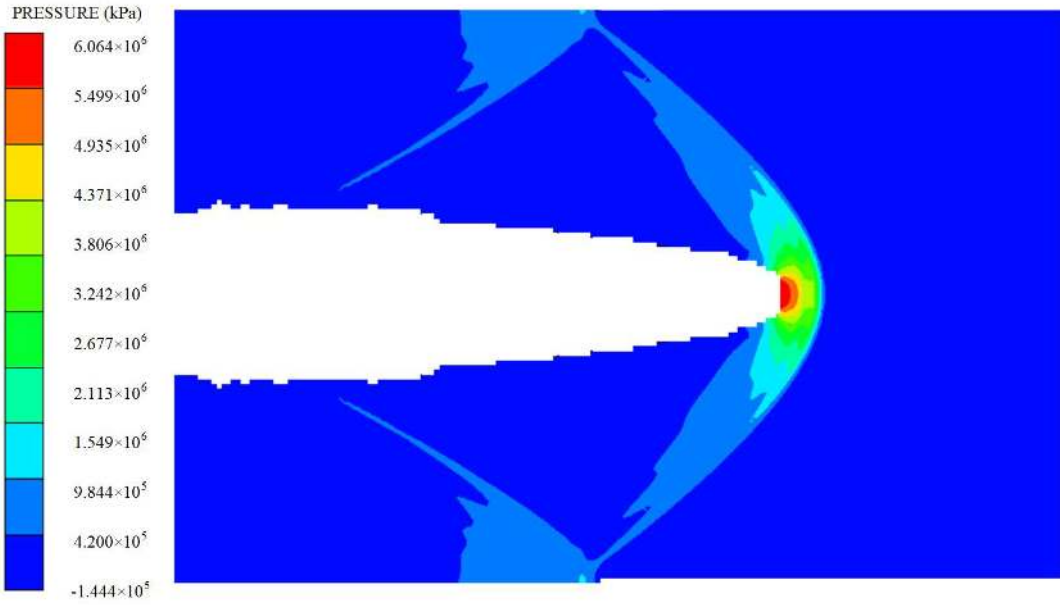


Figure 8 Comparison between simulation results and experimental results

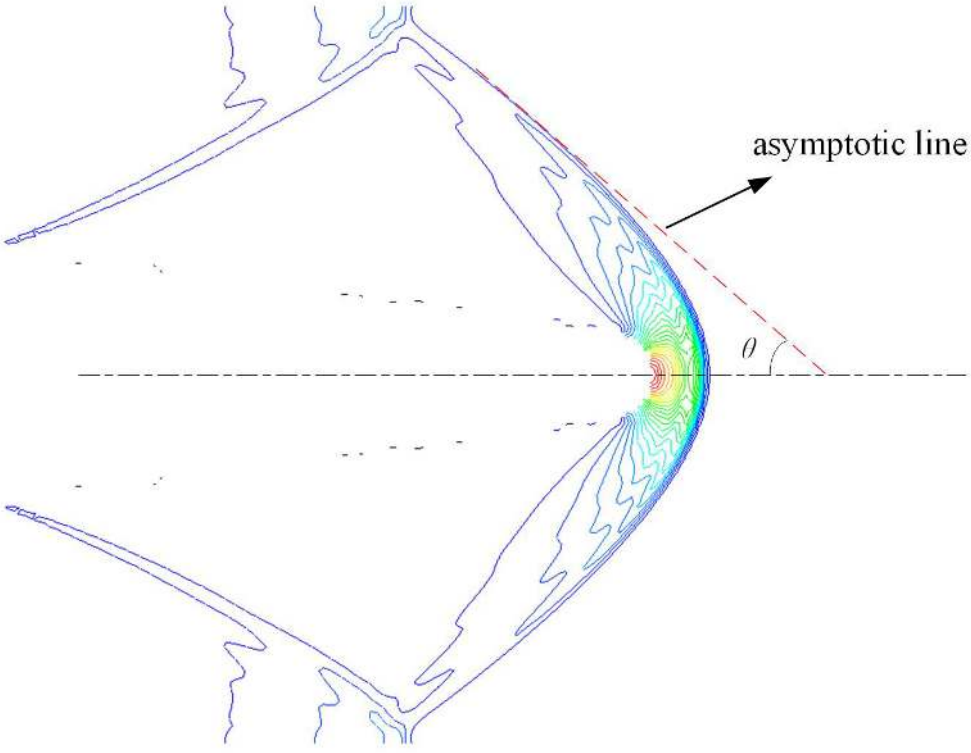
4.3 Simulation results

Taking the example of a projectile with a velocity of 4500 m/s and a diameter of 1.5 mm, the pressure distribution in water during the stable propagation of the shockwave is shown in Figure 9(a). As the projectile penetrates the water, it creates a shockwave. The oblique shockwave undergoes regular reflection on the inner wall of the cavity, forming a reflected shockwave. When the velocity of the penetrator remains constant, both shockwaves stably propagate forward

together. Figure 9 (b) shows the isobaric distribution of shockwave and reflected shockwave in water, where the dotted red line marked is the asymptotic line of the shockwave front, and the angle between it and the central axis is the cone angle of the shock wave front θ.



(a) Pressure distribution in water



(b) Isobaric distribution in water

Figure 9 Propagation of shockwave and reflected shockwave in water

Figure 10 depicts the shape of the shockwave and reflected shockwave in water during the penetration of a constant velocity projectile with a diameter of 1 mm into the liquid composite protective structure, at various velocities ranging from 4500 to 10500 m/s. The simulation results reveal that as the penetration velocity increases, the cone angle of the shockwave front gradually decreases.

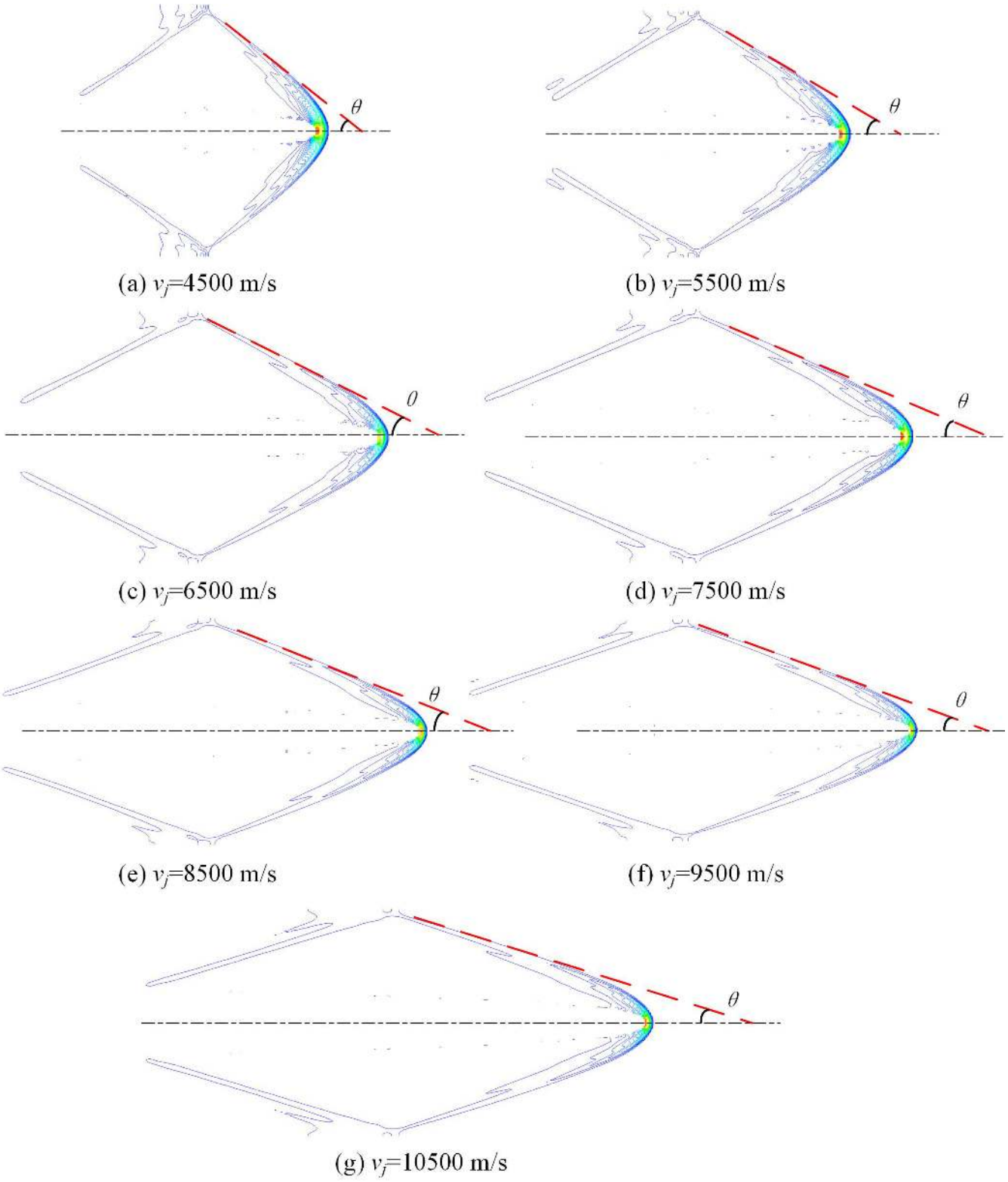


Figure 10 Shockwaves formed by projectile at different velocities

Figure 11 illustrates the shape of the shockwave and reflected shockwave in water when projectiles with varying diameters penetrate the liquid composite protective structure at a constant velocity of 6500 m/s. According to the simulation results, it can be observed that as the diameter of the projectile increases, the cone angle of the shockwave front gradually increases. Additionally, the curvature radius of the arc portion at the head of the shockwave also increases.

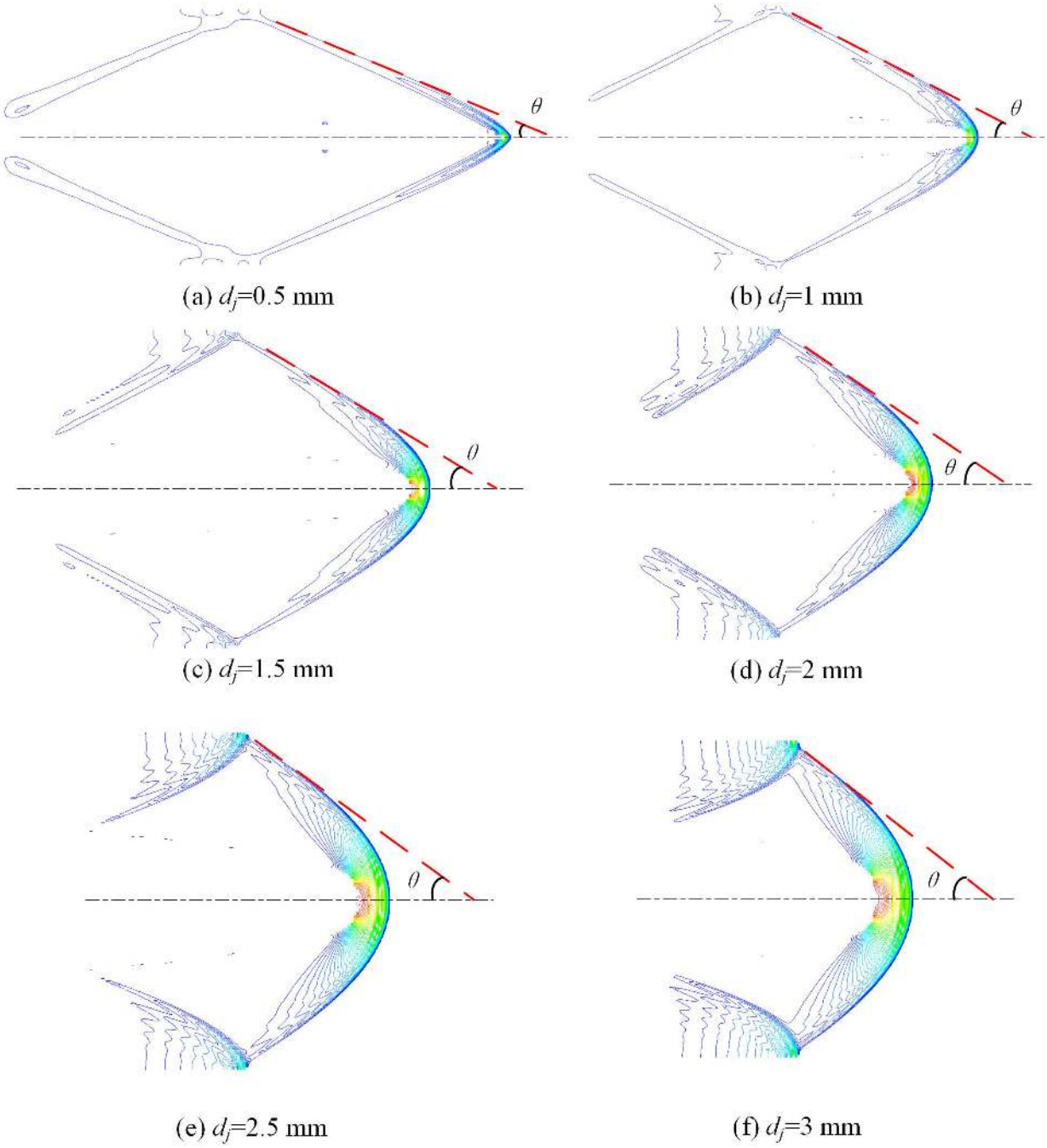


Figure 11 Shockwave in water formed by projectiles with different diameter

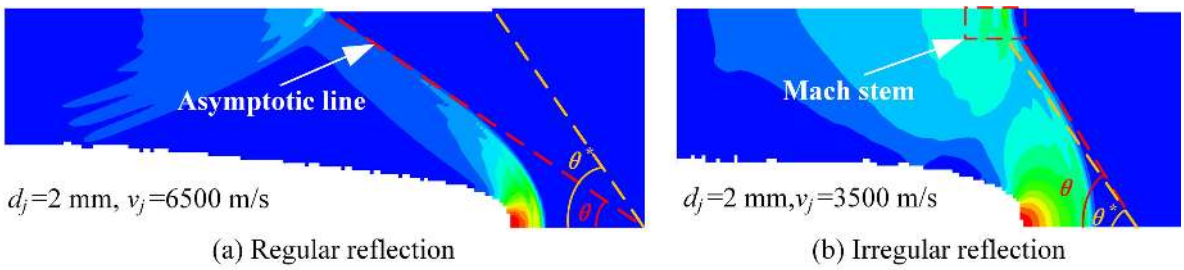


Figure 12 Distribution of shockwave pressure with different reflection types

Figure 12 demonstrates that when the shock incident angle surpasses the critical incident angle, the shockwave undergoes irregular reflection on the inner cavity wall, resulting in the formation of a Mach stem at the point of reflection.

By analyzing the simulation results, the distribution of both regular and irregular reflections of the shockwave on the inner cavity wall was obtained, as depicted in Figure 13.

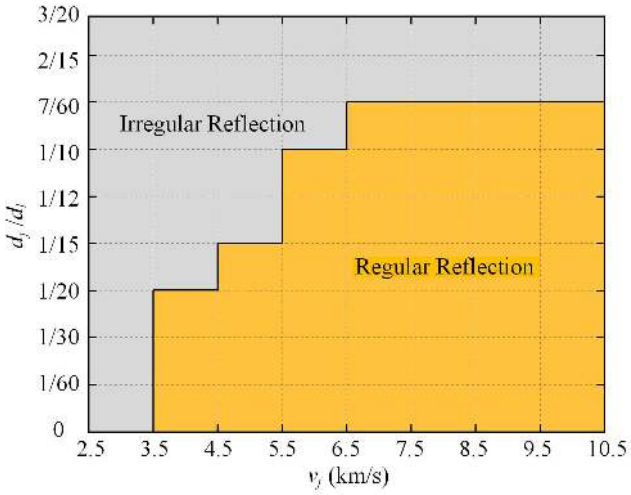


Figure 13 Distribution of shockwave reflection types

It can be observed that factors d_j/d_l and v_j play a significant role in determining whether the initial shockwave undergoes regular or irregular reflection on the inner cavity wall. When the normalized diameter d_j/d_l is too large or when the projectile velocity v_j is too low, the shockwave is more likely to undergo irregular reflection on the wall. This irregular reflection generates an adverse velocity component that hinders the radial convergence of liquid particles. In order to design a liquid composite protective structure effectively, it is desirable to avoid excessively large incident angles of the shockwave by altering the diameter of the liquid cavity. This is done to prevent irregular reflections from occurring. The subsequent analysis will focus only on the data related to shockwave incident angles smaller than the critical incident angle.

Figure 14 demonstrates the simulated values of the shockwave front cone angle and the calculated values of the Mach angle θ_t for different diameters and velocities of the projectile. It can be observed that the cone angles corresponding to the regular reflection of the shockwave are all within the critical angle calculated by equation (4). When the diameter of the projectile remains constant, the cone angle of the shockwave front gradually decreases as the velocity of the projectile increases, with a smaller decrease gradient. When the velocity of the projectile remains constant, the cone angle of the shockwave front increases with the increase in the projectile diameter. Additionally, the difference between the cone angle of the shockwave front and the Mach angle becomes more pronounced at lower velocities of the projectile.

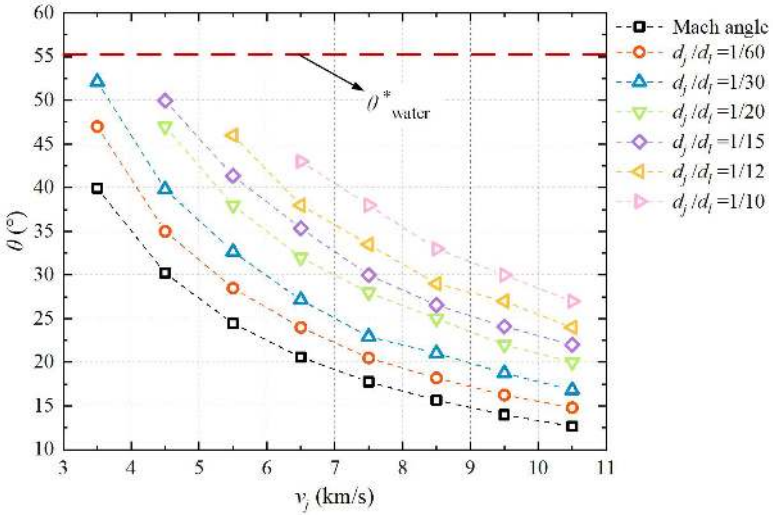


Figure 14 Variation trend of cone Angle of shockwave front with projectile velocity

The simulation results were normalized, and the normalized cone angle θ/θ_t was calculated for different normalized diameter d_j/d_l and projectile velocities v_j. The calculated values are presented in Table 7.

Table 7 Experiment parameters and result statistics

d_j/d_l	1/60	1/30	1/20	1/15	1/12	1/10
$v_j = 3.5$ km/s	1.177	1.305	—	—	—	—
$v_j = 4.5$ km/s	1.158	1.317	1.555	1.654	—	—
$v_j = 5.5$ km/s	1.166	1.336	1.555	1.691	1.882	—
$v_j = 6.5$ km/s	1.167	1.320	1.556	1.719	1.847	2.090
$v_j = 7.5$ km/s	1.153	1.290	1.575	1.688	1.885	2.138
$v_j = 8.5$ km/s	1.162	1.344	1.597	1.697	1.852	2.108
$v_j = 9.5$ km/s	1.162	1.341	1.572	1.722	1.929	2.144
$v_j = 10.5$ km/s	1.170	1.330	1.581	1.740	1.897	2.134
Average	1.164	1.323	1.57	1.702	1.882	2.123

By plotting the data from Table 7, the trend of the normalized cone angle θ/θ_t with varying projectile velocities can be observed, as depicted in Figure 15. The different colored dashed lines represent the average values of the normalized cone angle θ/θ_t corresponding to different normalized diameter d_j/d_l, while the red dashed line represents the ratio between the critical angle and the Mach angle $\theta^*_{\text{water}}/\theta_t$. It can be observed that for the same normalized diameter, when the projectile penetrates the liquid at different velocities, the relative error between the normalized cone angle and its average value is very small, ranging from 0.12% to 2.80%. This small relative error indicates that the normalized cone angle θ/θ_t can be considered as a fixed value for the same normalized diameter d_j/d_l.

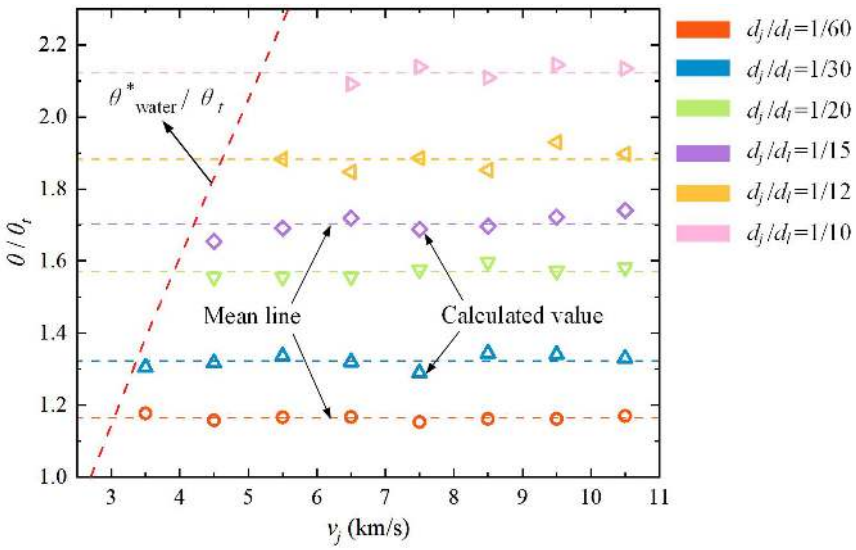


Figure 15 Variation trend of normalized cone angle versus projectile velocities

Therefore, when the cone angle of the incident shockwave front is within the range of $0 < \theta \leq \theta^*_{water}$, i.e., when the shockwave undergoes regular reflection on the inner cavity wall, the normalized cone angle θ/θ_t is solely a function of the normalized diameter d_j/d_l, as stated in equation (10).

Considering that as the normalized diameter d_j/d_l approaches zero, i.e., when the projectile diameter becomes infinitely small or the propagation distance of the shockwave becomes infinitely large, the cone angle of the shockwave front approximates the Mach angle (Held 1995), and we obtain the boundary condition

$$\lim_{\delta(d_j/d_l)\to 0} \frac{\theta}{\theta_t} = 1 \tag{17}$$

The average value of the normalized cone angle θ/θ_t for different normalized diameter d_j/d_l were fitted, and the fitting line is shown in Figure 16.

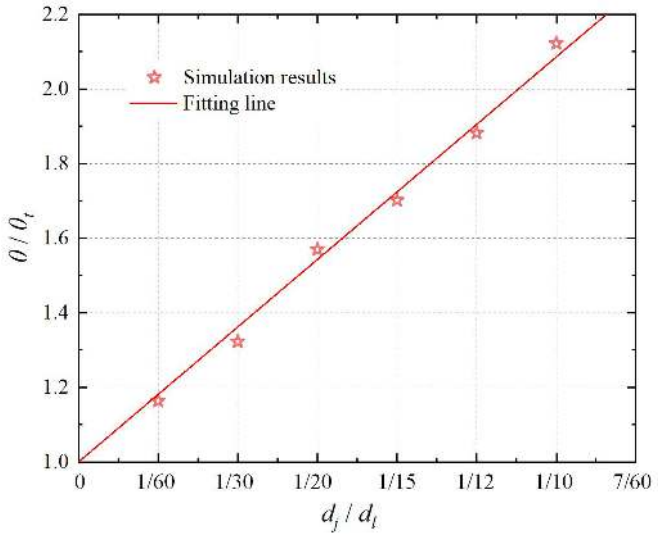


Figure 16 Trend of average value of normalized cone angle with respect to normalized diameter

Therefore, within the range of $0 < \theta \leq \theta^*$, the function relating the normalized cone angle θ / θ_t to the normalized diameter d_j/d_l can be expressed as follows:

$$\frac{\theta}{\theta_t} = f\left(\frac{d_j}{d_l}\right) = 10.8633\frac{d_j}{d_l} + 1 \tag{18}$$

Then, the formula for calculating the cone angle of the shockwave front is

$$\theta = \left(10.8633\frac{d_j}{d_l} + 1\right)\arcsin\left(\frac{c_l}{u}\right) = 10.8633\frac{d_j}{d_l}\arcsin\left(\frac{c_l}{u}\right) + \arcsin\left(\frac{c_l}{u}\right) \tag{19}$$

It can be seen that the cone angle of the shockwave front is composed of two terms, one of which is the Mach angle, and the other is a correction term related to the normalized diameter d_j/d_l. When the normalized diameter is large, the error of in approximating the cone angle of the shockwave front as the Mach angle is relatively large. However, as the normalized diameter approaches zero, the calculated value of the cone angle of the shockwave front becomes closer to the Mach angle.

5 CONCLUSION

In this study, dimensional analysis and numerical simulation were used to analyze the cone angle of the shockwave front during the penetration of a projectile into a liquid composite protective structure. The following conclusions were obtained:

1. In continuous medium, when the cone angle of the incident shockwave front is within the range of $0 < \theta \leq \theta^*$, the normalized cone angle θ/θ_t is solely a function of the normalized diameter d_j/d_l;

2. The formula for calculating the cone angle of the shockwave front is given as $\theta = \left(10.8633\frac{d_j}{d_l} + 1\right)\arcsin\left(\frac{c_l}{u}\right)$.

   When the diameter ratio is large, approximating the cone angle of the shockwave front as the Mach angle will result in a significant error. This error is related to the normalized diameter $\frac{d_j}{d_l}$ and can be expressed as $10.8633\frac{d_j}{d_l}$.

3. The use of the AUTODYN software and fluid-structure interaction algorithms can effectively simulate the propagation process of the shockwave during the supersonic penetration of a projectile into a liquid composite protective structure. The simulation results show a high level of agreement with experimental results.

4. The results of this study can be applied to the determination of the cone angle of shockwave front during the supersonic penetration of a projectile into liquid-filled structures, especially for cases where the propagation distance of the shockwave is relatively short.

5. In the next step, the relationship between the profile description of the bow part of the shockwave front and the parameters of the jet and the composite structure will be developed. This development aims to enhance the study of the propagation characteristics of the shockwave in liquid composite protective structures.

ACKNOWLEDGEMENT

This study is supported by the Jiangsu Province Graduate Research and Practice Innovation Program (grant number KYCX20_0308) and the National Natural Science Foundation of China (grant number 11602110).

Author's Contributions: Writing - original draft, You-er Cai; Test technical support, Xudong Zu, Qiangqiang Xiao, Zhengxiang Huang; Writing - review & editing, Yaping Tan, Xudong Zu, Xiaojun Shen, Xin Jia.

Editor: Marcílio Alves

References

Ansys Inc. Ansys explicit dynamics analysis guide. ANSYS 2022 R1. ANSYS Inc, 2022, USA.

Ben-Dor G. Shock Wave Reflection Phenomena. 2nd Edition. Berlin: Springer-Verlag Press, 2007.

Cai Y.E., Huang Z.X., Tan Y.P., Zu X.D., Shen X.J., Jia X. Influence of Strongly-Constrained Liquid-Filled Composite Armor on Stability of Incoming Shaped Charge Jet during Eccentric Penetration. Latin American Journal of Solids and Structures, 2022, 19. https://doi.org/10.1590/1679-78257098.

Cai Y.E., Zu X.D., Tan Y.P., Huang Z.X. Study on the Interference Process of Liquid Radial Reflux on the Stability of a Shaped Charge Jet. Applied Sciences, 2021, 11(17): 8044. https://doi.org/10.3390/app11178044.

Cao H., Sun B., Xu L., et al. Research on Armor Protection Technology. Beijing: Beijing Institute of Technology Press, 2019. (In Chinese)

Gao Z.Y., Huang Z.X., Guo M., et al. Analysis of Anti-Jet Penetration Performance of Diesel-Filled Sealed Structures. Journal of Vibration and Shock, 2016a, 35(14): 176-181. (In Chinese)

Gao Z.Y., Huang Z.X., Guo M., et al. Theoretical Study of a Diesel-Filled Airtight Structure Unit Subjected to Shaped Charge Jet Impact. Propellants, Explosives, Pyrotechnics, 2016b,41:62-68. https://doi.org/10.1002/prep.201500137.

Gu, Y., Wang, J., Li, H., Tang, K., & Liu, L. (2022). Formation characteristics and penetration performance of an underwater shaped charge jet. Ocean Engineering, 258, 111695. https://doi.org/10.1016/j.oceaneng.2022.111695.

Guo M., Zu X., Huang Z., Shen X.J. Mechanism of Hermetic Single-Cell Structure Interfering with Shaped Charge Jet. Latin American Journal of Solids and Structures, 2018, 15. https://doi.org/10.1590/1679-78254977.

Guo M., Zu X., Shen X.J., Huang Z. Study on Liquid-Filled Structure Target with Shaped Charge Vertical Penetration. Defence Technology., 2019, 15, 861–867. https://doi.org/10.1016/j.dt.2019.05.003.

Held M. Verification of the Equation for Radial Crater Growth by Shaped Charge Jet Penetration. International Journal of Impact Engineering, 1995, 17(1-3): 387-398. https://doi.org/10.1016/0734-743X(95)99864-N.

Held M., Huang N.S., Jiang D., et al. Determination of the Crater Radius as a Function of Time of a Shaped Charge Jet that Penetrates Water. Propellants, Explosives, Pyrotechnics, 1996, 21(2): 64-69, https://doi.org/10.1002/prep.199602 10203.

Huang Z. Shaped Charge Theory and Practice. Beijing: Beijing Institute of Technology Press, 2014. (In Chinese)

Johnson GR, Cook WH. A constitutive model and data for metals subjected to large strains, high strain-rates and high temperatures. In: Proceedings of the 7th International Symposium on Ballistics; 1983. p. 541–547.

Kawamura R., Saito H. Reflection of Shock Waves-1 Pseudo-Stationary Case. J. Phys. Soc. Japan, 1956, 11: 584-592. https://doi.org/10.1143/JPSJ.11.584.

Mach E. Uber den Verlauf von Funkenwellen in der Ebene und im Raume. Sitzugsbr Akad Wiss Wien, 1878, 78: 819-838.

Shi, J., Huang, Z., Zu, X., and Xiao Q. Cohesiveness and penetration performance of jet: Theoretical, numerical, and experimental studies. International Journal of Impact Engineering 175 (2023): 104543. https://doi.org/10.1016/j.ijimpeng.2023.104543.

Steinberg, D. J., Cochran S. G., and Guinan M. W. A constitutive model for metals applicable at high strain rate. Journal of Applied Physics 51.3 (1980): 1498-1504.

Tan Y., Jia X., Huang Z., Cai Y., Zu X. Effect of Liquid Parameters on Protective Performance of a Liquid Composite Target Subjected to Jet Impact. In Proceedings of the 15th Hypervelocity Impact Symposium, Destin, FL, USA, 14–19 April 2019.

Vasilev E.I., Elperin T., Ben-Dor G. Analytical reconsideration of the von Neumann paradox in the reflection of a shock wave over a wedge. Physics of Fluids, 2008, 20(4): 046101. https://doi.org/10.1063/1.2896286.

White J.J., Wahll M.J. Shaped charge jet interactions with liquids. Proceedings of the 6th International Symposium on Ballistics, ADPA Orlando, Florida, 1981: 554-561.

Williams AG, Dhingra J. IHSTM Jane's® weapons: ammunition. London, UK: IHS JANES; 2016.

Yang Y., Jiang Z., Hu Z. Research Progress on Shock Wave Reflection Phenomena. Advances in Mechanics, 2012, 42(2): 141-161. (In Chinese)

Yang, G., Fan, Y., Wang, G., Cui, X., Li, Q., Leng, Z., and Deng, K. (2023). Mitigation effects of air-backed RC slabs retrofitted with CFRP subjected to underwater contact explosions. Ocean Engineering, 267, 113261. https://doi.org/10.1016/j.oceaneng.2022.113261.

Zhang Q., Hao F., Li Y., et al. Damage and Protection of Vehicles and Personnel under Explosive Impact Loads. Mechanics in Engineering, 2014, 36(05): 527-539. (In Chinese)

Zhang X., Zu X., Huang Z., et al. Interference Characteristics Analysis of Single-Cell Structures Filled with Liquid on Jet. Explosions and Shock Waves, 2017, 37(06): 1101-1106. (In Chinese)

Zhang Z., Zhao B., Zhang R., et al. Fundamentals of Armor Protection Technology. Beijing: Ordnance Industry Press, 2000: 118-167. (In Chinese)

Zhang, Z., Li H., Wang L., et al. Protection mechanism of underwater double-hull coated with UHMW-PE subjected to shaped charge. Ocean Engineering 272 (2023): 113842. https://doi.org/10.1016/j.oceaneng.2023.113842.

Zhu, W., Huang, G. Y., Guo, Z. W., Lai, W., and Feng, S. S. (2019). Ballistic penetration of bi-layer structures with water container and fiber composite: Effects of the container position. Composite Structures, 227, 111320. https://doi.org/10.1016/j.compstruct.2019.111320.

Żochowski P, Warchoł R. Experimental and numerical study on the influence of shaped charge liner cavity filing on jet penetration characteristics in steel targets. Defence Technology, 2023, 23: 60-74. https://doi.org/10.1016/j.dt.2022.09.007.

Zu X., Dai W., Huang Z., Yin X. Effects of Liquid Parameters on Liquid-Filled Compartment Structure Defense against Metal Jet. Materials, 2019, 12, 1809. https://doi.org/10.3390/ma12111809.

Zu X.D., Huang Z.X., Guan Z.W., et al. Influence of a Liquid-Filled Compartment Structure on the Incoming Shaped Charge Jet Stability. Defence Technology, 2021, 17(2): 571-582. https://doi.org/10.1016/j.dt.2020.03.009.